

Triadic percolation in computer virus spreading dynamics

Jie Gao(高杰), Jianfeng Luo(罗建锋), Xing Li(李星), Yihong Li(李毅红), Zunguang Guo(郭尊光), and Xiaofeng Luo(罗晓峰)

Citation: Chin. Phys. B, 2025, 34 (**2**): 028701. DOI: 10.1088/1674-1056/ad9ff8
Journal homepage: http://cpb.iphy.ac.cn; http://iopscience.iop.org/cpb

What follows is a list of articles you may be interested in

A Weibo local network growth model constructed from the perspective of following-followed

Fu-Zhong Nian(年福忠) and Ran-Qing Yao(姚然庆)
Chin. Phys. B, 2024, 33 (**12**): 128702. DOI: 10.1088/1674-1056/ad84c4

Effects of individual heterogeneity on social contagions

Fu-Zhong Nian(年福忠) and Yu Yang(杨宇)
Chin. Phys. B, 2024, 33 (**5**): 058705. DOI: 10.1088/1674-1056/ad225e

Dynamics of information diffusion and disease transmission in time-varying multiplex networks with asymmetric activity levels

Xiao-Xiao Xie(谢笑笑), Liang-An Huo(霍良安), Ya-Fang Dong(董雅芳), and Ying-Ying Cheng(程英英)
Chin. Phys. B, 2024, 33 (**3**): 038704. DOI: 10.1088/1674-1056/ad1176

Studying the co-evolution of information diffusion, vaccination behavior and disease transmission in multilayer networks with local and global effects

Liang'an Huo(霍良安) and Bingjie Wu(武兵杰)
Chin. Phys. B, 2024, 33 (**3**): 038702. DOI: 10.1088/1674-1056/ad0114

Bio-inspired environmental adaptability of swarm active matter

Yangkai Jin(金阳凯), Gao Wang(王高), Daming Yuan(袁大明), Peilong Wang(王培龙), Jing Wang(王璟), Huaicheng Chen(陈怀城), Liyu Liu(刘雳宇), and Xingjie Zan(昝兴杰)
Chin. Phys. B, 2023, 32 (**8**): 088703. DOI: 10.1088/1674-1056/acd688

Triadic percolation in computer virus spreading dynamics

Jie Gao(高杰)[1], Jianfeng Luo(罗建锋)[1], Xing Li(李星)[1], Yihong Li(李毅红)[1], Zunguang Guo(郭尊光)[2], and Xiaofeng Luo(罗晓峰)[1,†]

[1] *School of Mathematics, North University of China, Taiyuan* 030051, *China*
[2] *Department of Science, Taiyuan Institute of Technology, Taiyuan* 030008, *China*

(Received 15 October 2024; revised manuscript received 4 December 2024; accepted manuscript online 17 December 2024)

In recent years, the threats posed by computer viruses have become increasingly diverse and complex. While classic percolation theory provides a novel perspective for analyzing epidemics and information dissemination, it fails to capture the temporal dynamics of these systems and the effects of virus invasion and governmental regulation. Triadic percolation theory, a recent advancement, addresses these limitations. In this paper, we apply this new percolation mechanism to model the diffusion of computer viruses, deriving a precise mathematical formulation of the triadic percolation model and providing an analytical solution of the triadic percolation threshold. Additionally, we investigate the impact of nonlinear transmission probability characteristics on virus propagation. Numerical simulations demonstrate that reducing the network's average degree (or the positive regulation) or increasing regulatory interventions raises the outbreak threshold for computer viruses while decreasing their final size. Moreover, the study reveals that nonlinear transmission probabilities result in an increased number of solutions for the final size of the computer viruses. Our findings contribute new insights into controlling the spread of computer viruses.

Keywords: triadic percolation, percolation threshold, nonlinear transmission probability, final size

PACS: 87.23.Kg, 05.45.–a, 02.60.Cb

DOI: 10.1088/1674-1056/ad9ff8 **CSTR:** 32038.14.CPB.ad9ff8

1. Introduction

Computer viruses are malevolent software programs intended to damage computer systems. They can replicate and spread across networks, causing damage by stealing data, destroying files, altering registries, and more.[1,2] For instance, the "CIH" virus emerged in 1998 and disseminated swiftly, capable of destroying computer hardware and causing considerable disruption. In 1999, the "Melissa" virus spread via email, contaminating 15% to 20% of the world's business computers and causing substantial economic losses. In 2006, the "Panda Virus (WhBoy)" evaded anti-virus software, spreading automatically and causing damage amounting to hundreds of millions of dollars. More recently, the "WannaCry" and "Ransom" viruses have wreaked havoc globally, encrypting victims' files and extorting ransom payments, severely impacting medical systems and enterprises in numerous countries. To effectively inhibit the spread of computer viruses over the internet, it is always crucial to establish mathematical models, explore the spread behavior of these viruses, and develop effective control strategies.

Percolation theory,[3–7] a pivotal concept in statistical physics, was introduced by Hammersley[8] in 1957. This theory holds significant value and potential applications in network science, categorizing percolation models into two types: site-percolation and bond-percolation.[9,10] These models simulate scenarios where nodes or edges in a network are occupied with a certain probability, thereby simplifying the dynamic processes in complex networks and providing a novel perspective for analyzing the mechanisms of epidemic[11–14] and information[15,16] outbreaks. Specifically, percolation theory provides a framework for the susceptible–infected–removed (SIR) model, enabling the quantitative evaluation of epidemic thresholds, the final scale of outbreaks, and other critical epidemic parameters. In this context, the occupancy of edges directly corresponds to the successful transmission of epidemic among individuals, while the emergence of the giant component signifies the percolation threshold, indicating a widespread outbreak. Additionally, percolation models can assess the efficacy of immunization,[17–21] providing a solid theoretical foundation for formulating scientific and reasonable prevention and control measures. However, classic percolation theory does not adequately capture the dynamic changes in the network over time. In response, triadic percolation has been introduced to bridge this gap. Sun *et al.*[22] introduced the higher-order interaction mechanism of triadic interaction, wherein the regulatory effect of one network node influences the interactions between the other two nodes. These regulations can either promote or inhibit interactions, thereby providing a more accurate representation of the complexity of interactions. Milláné *et al.*[23] further revealed the multi-stability characteristics of triadic percolation, highlighting that the giant component undergoes significant topo-

[†]Corresponding author. E-mail: luoxiaofeng@nuc.edu.cn

© 2025 Chinese Physical Society and IOP Publishing Ltd. All rights, including for text and data mining, AI training, and similar technologies, are reserved.

logical changes over time. It is evident that triadic percolation theory not only captures temporal dynamics but also considers intricate patterns of promotional and inhibitory interactions. Drawing upon these advancements, we employ triadic percolation theory to investigate the dissemination of computer viruses.

Currently, based on large-scale data,[24–26] researchers have clarified the nature, rules, and trends of computer virus activities, visualizing the behavioral patterns of viruses and their influence on network security. Recognizing the similarities between epidemiological diseases dynamics and computer viruses propagation,[27–30] models for the spread of computer viruses are frequently developed using epidemiological theories.[31–35] Can *et al.*[36] studied the spread of computer viruses on complex networks, taking into account the combined effects of network topology and mobile storage media. Mario[37] modeled the spread of computer virus as a stochastic differential game based on the two-dimensional (2D) Kermack–McKendrick epidemic model. Yang *et al.*[38] explored the impact of isolation strategies and temporary immunity delays by developing an SIQRS model for the spread of computer virus, incorporating a nonlinear infection rate and dual time delays. Zhu *et al.*[39] comprehensively considered both the node's self-information and the role of the location information of neighboring nodes, proposed an improved global structure model, and simulated the propagation process of the real network. Derya *et al.*[40] proposed an optimal control strategy to mitigate the harm caused by computer virus based on the fractional-order SEIR epidemiological model. However, these studies have primarily concentrated on the dynamics of spread while neglecting government regulation, the self-positive regulation of computer viruses, and the nonlinear characteristics of transmission probability.

Motivated by the three aspects above, we derived the triadic percolation model, considering the nonlinear characteristics of transmission probability, analytically determined the percolation threshold. We further simulated the effects of varying transmission probabilities and regulations (e.g., government regulation, self-regulation of computer virus) on final spreading dynamics. Our research indicates that a denser network and stronger positive regulation lead to a larger final size of virus spread, while a smaller negative regulation also contributes to an increased final size. Under consistent network density and regulation, the final size of the nonlinear model is significantly smaller. These results provide deeper insights into understanding the spreading dynamics of computer virus and the impact of government regulation.

The structure of this paper is as follows. In Section 1, we provide an overview of the research background. In Section 2, we derive the triadic percolation model of computer virus spreading based on the triadic percolation process and the probability generating function method, incorporating the nonlinear characteristics of transmission probability. In Section 3, we analyze and calculate the percolation threshold of the triadic percolation model, providing the theoretical form of the threshold and examining the impact of various parameters and nonlinear properties on it. In Section 4, we use MATLAB simulations to explore the triadic percolation model of computer virus spreading, illustrating the relationship between final solutions and each parameter. Finally, in Section 5, we summarize the results of this paper.

2. Triadic percolation for computer virus spreading

Triadic percolation is essentially to describe the percolation phenomenon on the higher-order network with triadic interactions among nodes in structural and regulatory networks.[22] It can predict the proportion of nodes in the giant component which are active under the regulatory interactions.

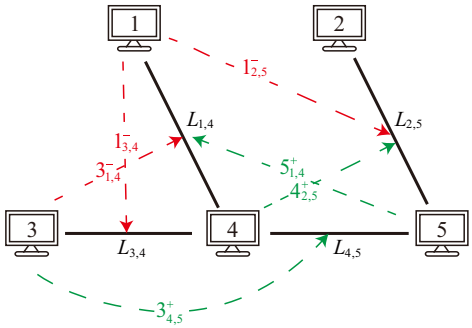


Fig. 1. A simple initial network of computer connections consisting of the structural and regulatory network. The structural network $\mathcal{A}(V,E)$ consists of a collection of computers $1,2,3,4,5$ connected by the structural interactions $L_{1,4}$, $L_{3,4}$, $L_{2,5}$, $L_{4,5}$ (black solid lines). The regulatory network $\mathcal{B}(V,W)$ is a bipartite, signed network between the set of computers $1,2,3,4,5$ and the set of structural interactions $L_{1,4}$, $L_{3,4}$, $L_{2,5}$, $L_{4,5}$, with computers' regulatory links, either positive $3^+_{4,5}$, $4^+_{2,5}$, $5^+_{1,4}$ (green dotted lines) or negative $1^-_{3,4}$, $1^-_{2,5}$, $3^-_{1,4}$ (red dotted lines).

Higher-order networks with triadic interactions are modeled as a combination of a structural network and a regulatory network. The nodes in both networks are identical, but serve different functions. Specifically, certain structural nodes also fulfill regulatory functions. Triadic interactions depict the mechanism by which a structural node with regulatory function (termed to a regulatory node) regulates the interaction between two other structural nodes (structural interaction). For example, as shown in Fig. 1, structural node 1 regulates the interaction $L_{3,4}$ between structural nodes 3 and 4 through the regulatory link $1^-_{3,4}$. This configuration, comprising nodes 1, 3, 4, along with the regulatory link $1^-_{3,4}$ and structural interaction $L_{3,4}$, constitutes a triadic interaction. One structural interaction is active indicates that this structural link exists and transmits the virus. The activity of this interaction between these two structural nodes is contingent upon the regulatory node in the triadic interaction. If the regulatory node is active and has

a promoting role, the structural interaction it regulates is also active. If the regulatory node is active but has a inhibiting role, or if the regulatory node is inactive, the structural interaction it regulates is inactive. Ultimately, the activity of a regulatory node is determined by its presence in the giant component.

In what follows, we will further elaborate on the triadic percolation mechanism in the context of computer virus spreading.

2.1. Triadic percolation mechanism for computer virus spreading

In the context of computer virus dissemination, the concept of triadic percolation is applied within a higher-order network framework. Initially, let V denote the set of the nodes common to both the structural network and the regulatory network. The set W represents the regulatory links in the regulatory network, which are functional only when the node connected to them is active. E signifies the set of the structural links in the structural network. In the regulatory network $\mathcal{B}(V,W)$ of computer virus spreading, an active node correspond to a computer capable of playing a regulatory role (either positive or negative), while an inactive node represents a computer that lacks such a capability. A positive regulatory role refers to a computer manipulated by malicious actors to facilitate virus dissemination, whereas a negative role pertains to computers that mitigate transmission through various preventive measures. In the structural network $\mathcal{A}(V,E)$ of computer virus spreading, an active node indicates an infected computer while an inactive node signifies one that remains uninfected. In other words, we assume that only infected computers can exert regulatory influence. An active or inactive structural interaction respectively corresponds to one interaction that is either capable or incapable of transmitting the virus between the interconnected computers at its endpoints. The probability associated with transmission via an active structural interaction is denoted as $p(T)$. Given existing defense mechanisms, it is assumed that infected computers in small connected component or isolated infected computers recover to susceptible computers with a probability of 1.

The spread process of computer virus is governed by the triadic percolation mechanism within the specified structural network $\mathcal{A}(V,E)$ and regulatory network $\mathcal{B}(V,W)$. In the subsequent sections, we provide a detailed illustration of this triadic percolation mechanism as it pertains to virus spread across both regulatory and structural networks, as depicted in Fig. 2, which is based on a simplified initial higher-order network shown in Fig. 1. Additionally, Table 1 outlines the iterative algorithm for each time step $t \geq 1$ corresponding to Fig. 2.

Table 1. The triadic percolation mechanism for computer virus spreading.

	General iterative rule
Step 1	Determine the activity of each computer at time t. The computer is active if it is connected to the giant component of the structural network, or otherwise inactive. They all depend on the activity configuration of a given structural connection at time $t-1$.
Step 2	Determine the activity of each structural interaction at time t. One structural interaction is inactive if it is connected to one or more active computer with negative regulator role and/or that are not connected to any active computer with positive regulatory role. One structural interaction is active when the positive regulatory computers regulating this interaction activate or the negative regulatory computers inactivates. Virus spread with probability $p(T)$ on those active structural interactions. They all depend on the activities of the computers regulating it in step 1 at time t.

To gain a clear understanding of the triadic percolation mechanism for computer virus spreading as presented in Table 1, figure 2 provides a specific example with $p(T) = 1$. At the initial time $t = 1$, the structural network $\mathcal{A}(V,E)$ and the regulatory network $\mathcal{B}(V,W)$ are established in step 1. We assume that all computers and structural interactions are active, but not all are infected initially, with computer 4 being the only infected one. Subsequently, based on this initial setting, the triadic percolation process for the computer virus is initiated. In step 2, the structural interactions $L_{1,4}$, $L_{3,4}$, $L_{2,5}$ become inactive due to the negative regulatory links $3^{-}_{1,4}$, $1^{-}_{3,4}$, $1^{-}_{2,5}$. Meanwhile, structural interaction $L_{4,5}$ remains active according to the presence of the positive regulatory link $3^{+}_{4,5}$. At the time $t = 2$, computer 5 is infected by computer 4 through the active structural interaction $L_{4,5}$. Computers 1, 2, and 3 are isolated and deactivated, since the structural interactions $L_{1,4}$, $L_{3,4}$, $L_{2,5}$ are inactivated at the time $t = 1$, meaning these three computers are not infected by computer 4. Consequently, in step 2, the negative regulatory links $3^{-}_{1,4}$, $1^{-}_{3,4}$, $1^{-}_{2,5}$ emerging from computers 1, 2, and 3 do not work, leading to the reactivation of the structural interactions $L_{1,4}$, $L_{3,4}$, $L_{2,5}$. The positive regulatory link $3^{+}_{4,5}$ also inactivates emerging from computer 3, causing the structural interaction $L_{4,5}$ to become inactive. At the time $t = 3$, computers 1 and 3 are infected by computer 4 through the active structural interactions $L_{1,4}, L_{3,4}$. Computer 2 remains virus-free and computer 5 recovers to the virus-free state as they are part of a small connected component. In step 2, the structural interaction $L_{1,4}$ becomes inactive

due to the presence of the negative regulatory link $3^{-}_{1,4}$, while the structural interactions $L_{3,4}$, $L_{2,5}$ become inactive because of the negative regulatory links $1^{-}_{3,4}$ and $1^{-}_{2,5}$. The structural interaction $L_{4,5}$ becomes active again as link $3^{+}_{4,5}$ becomes reactive. At the time $t = 4$, according to the activity of each structural interactions at the time $t = 3$, computers 1, 2, and 3 are inactivated again and return to the virus-free state. Computer 5 is infected again by computer 4.

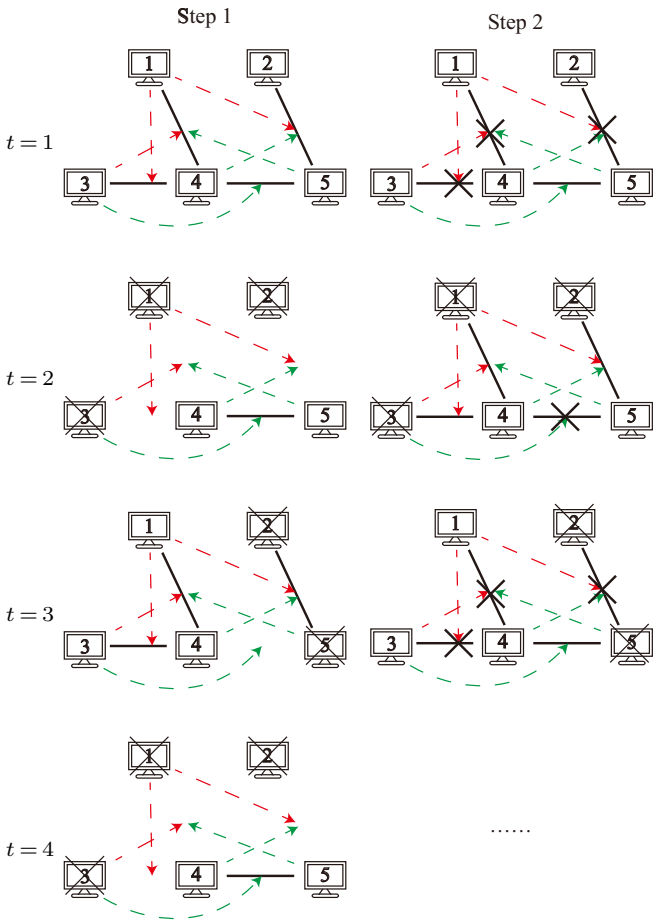


Fig. 2. Schematic diagram of triadic percolation process of computer virus spreading for the network given an initial state as shown in Fig. 1. To clearly understand, we assume that $p(T) = 1$. This visualization captures the dynamical behavior of the triadic percolation process for computer virus spreading within the given network structure.

In the context we described, $p(T)$ represents the transmission probability of computer virus through an active structural interaction, which is a function of the natural transmission probability (in the absence of any intervention), denoted as T. However, during the initial stage of computer virus spreading, the transmission takes place with a probability equivalent to T, attributable to the lack of effective antivirus software. As the virus's impact intensifies, government interventions are escalated, encompassing enhancements in anti-virus software and intensified information monitoring. Consequently, the transmission probability $p(T)$ might manifest a nonlinear relationship with the natural transmission probability T.[41,42] In accordance with the aforementioned instructions, we conduct an exploration of two types of functions: linear and nonlinear,[43] as depicted in Fig. 3. Subsequently,we analyze the impact of nonlinear transmission probability on the threshold and steady state of the triadic percolation.

(i) The linear relationship: $p(T) = (1-\alpha)T$.

A linear relationship exists between the transmission probability $p(T)$ and the natural transmission probability T, with this relationship being determined by the factor $1-\alpha$. The parameter α, where $\alpha \in [0,1)$, reflects the intensity of prevention and control measures. As the control intensity increases, the transmission probability $p(T)$ decreases linearly in relation to the natural transmission probability T.

(ii) The nonlinear relationship: $p(T) = CT/(DT+1)$.

A nonlinear relationship exists between the transmission probability $p(T)$ and the natural transmission probability T. The constants C and D determine the shape of the curve and characterize the intensity of the control measures. Specifically, a smaller value of C and a larger value of D indicates stronger control measures. This nonlinear relationship implies that the transmission probability $p(T)$ exhibits a saturation effect as the intensity of control measures increases relative to the natural transmission probability (see Fig. 3).

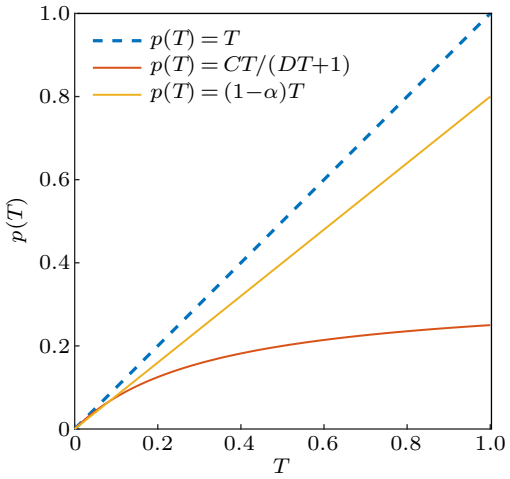


Fig. 3. The relation between the transmission probability $p(T)$ and the natural transmission probability T without intervention measures. Here, the blue dashed line represents the natural transmission probability, the red and yellow solid line represents the transmission probability under linear and nonlinear influence, respectively. The values of the constants satisfy $\alpha = 0.2$, $C = 1$, and $D = 3$.

In this section, we give the triadic percolation contagion mechanism for computer virus spreading. In what follows, according to this mechanism, we provide the mathematical derivation of the triadic percolation model.

2.2. Mathematical derivation of triadic percolation model for computer virus spreading

Inspired by the work in Ref. [16], we give the probability generating functions of the distributions of degree $p(k)$, excess degree $q(k)$ for each computer and the positive/negative

regulatory degree $\hat{P}_{\pm}(\hat{\kappa}^{\pm})$ for each structural interaction. Subsequently, leveraging the description of the triadic percolation mechanism, we mathematically derive the triadic percolation model for computer virus spreading in combination with schematic diagrams in Figs. 4 and 5.

2.2.1. Probability generating function

In the structural network, the probability that a randomly selected computer has k neighboring computers is denoted as $p(k)$, where $p(k) = N_k/N$. Here, N_k and N represent the number of computers with degree k and the total number of computers in the network. The generating function of the degree distribution of a computer in a structural network is defined as

$$G_0(x) = \sum_k p(k) x^k, \tag{1}$$

which informs all degree distribution information of the structural network as follows:

$$p(k) = \frac{1}{k!}\frac{\mathrm{d}^{\mathrm{k}} G_0}{\mathrm{d}x^k}|_{x=0}. \tag{2}$$

The average degree $\langle k\rangle$ of the structural network satisfies: $\langle k\rangle = \sum_k kp\langle k\rangle = G_0{}'(1)$.

The excess distribution $q(k)$ represents that a computer of excess degree k is reached along a randomly chosen structural interaction. The generating function of the excess distribution $q(k)$ in the structural network is defined as

$$G_1(x) = \sum_k \frac{(k+1)p(k+1)}{\langle k\rangle} x^k = \sum_k q(k) x^k. \tag{3}$$

In the regulatory network, the probability that a randomly selected structural interaction possesses $\hat{\kappa}^{\pm}$ positive (negative) regulatory links is denoted as $\hat{P}_{\pm}(\hat{\kappa}^{\pm})$, where $\hat{P}_{\pm}(\hat{\kappa}^{\pm}) = \hat{N}_{\hat{\kappa}^{\pm}}/\hat{N}$. Here, $\hat{N}_{\hat{\kappa}^{\pm}}$ and $\hat{N}$ represent the number of structural interactions with positive (negative) regulatory links $\hat{\kappa}^{+}$ ($\hat{\kappa}^{-}$) and the total number of structural interactions. The corresponding generating function of the regulatory link distribution of the structural interaction is defined as

$$G_0^{\pm}(x) = \sum_{\hat{\kappa}^{\pm}} \hat{P}_{\pm}\left(\hat{\kappa}^{\pm}\right) x^{\hat{\kappa}^{\pm}}. \tag{4}$$

The average degree $\langle\hat{\kappa}^{\pm}\rangle$ of the structural interactions satisfies: $\langle\hat{\kappa}^{\pm}\rangle = \sum_{\hat{\kappa}^{\pm}} \hat{\kappa}^{\pm}\hat{P}_{\pm}(\hat{\kappa}^{\pm}) = G_0^{\pm\prime}(1)$.

2.2.2. Mathematical derivation of the model

Based on the degree distribution previously discussed, we provide the detailed mathematical derivation of model. We first introduce the variables $P_L^{(t)}$, $R^{(t)}$, and $u^{(t)}$ of triadic percolation for computer virus. $P_L^{(t)}$ represents the probability that a randomly selected structural interaction is active and transmits the virus at the time t. $R^{(t)}$ and $u^{(t)}$ refer to the probabilities that a randomly selected computer is infected at the time t (i.e., the giant component size at the time t) and the probability that, along a randomly chosen interaction, a virus-free computer is reached at the time t, respectively. Subsequently, we illustrate $P_L^{(t)}$, $R^{(t)}$, and $u^{(t)}$ using schematic diagrams Figs. 4 and 5.

As described above in the triadic percolation mechanism, the structural interaction is considered active when it simultaneously satisfies the following two parts. On one hand, the negative regulatory links connected to this structural interaction must be inactive. This implies that the computers to which these negative regulatory links are connected are virus-free. For example, as shown in Fig. 4, in the first row, the structural link in all cases has no negative regulatory links. In the subsequent rows; second, third, fourth, and so on, the structural interaction in all cases has no active negative regulatory links. Although it is connected to one, two and three negative regulatory links, all these negative regulatory links are connected to the virus-free computers. This part can be mathematically expressed as $G_0^{-}(1-R^{(t)})$. On the other hand, at least one of the positive regulatory links connected to this structural interaction is active, that is, at least one of the computers connected to this positive regulatory link is infected. For example, as shown in Fig. 4, in the first column, the structural interactions have only a positive regulatory link and this link is active since connected to the infected computers. In the second and third columns, the structural interaction has two positive regulatory links. In the second column, one of these two positive regulatory links is active because it is connected to an infected computer and the other is inactive as it is connected to a virus-free computer. In the third column, both of these two positive regulatory links are connected to infected computers. In the fourth, fifth, and sixth columns, the structural interaction has three positive regulatory links. Among these links, in each of the three columns respectively, one, two, or three of them are active because they are connected to infected computers. The inactive cases are similar to the above descriptions, all of them are connected to virus-free computers. This part can be written as $1-G_0^{+}(1-R^{(t)})$. The above two parts ensure that the structural interaction is active. Lastly, one active structural interaction transmits computer virus with probability $p(T)$. Therefore, the probability $P_L^{(t)}$ that a randomly selected structural interaction is active and transmits the virus at the time t reads as

$$\begin{aligned} P_L^{(t)} &= p(T)\sum_{\hat{\kappa}^{-}} \hat{P}_{-}\left(\hat{\kappa}^{-}\right)\binom{\hat{\kappa}^{-}}{\hat{\kappa}^{-}}\left(1-R^{(t)}\right)^{\hat{\kappa}^{-}} \\ &\quad\times\left[1-\sum_{\hat{\kappa}^{+}} \hat{P}_{+}\left(\hat{\kappa}^{+}\right)\binom{\hat{\kappa}^{+}}{\hat{\kappa}^{+}}\left(1-R^{(t)}\right)^{\hat{\kappa}^{+}}\right] \\ &= p(T)\sum_{\hat{\kappa}^{-}} \hat{P}_{-}\left(\hat{\kappa}^{-}\right)\left(1-R^{(t)}\right)^{\hat{\kappa}^{-}} \end{aligned}$$

$$\times\left[1-\sum_{\hat{\kappa}^+}\hat{P}_+\left(\hat{\kappa}^+\right)\left(1-R^{(t)}\right)^{\hat{\kappa}^+}\right]$$
$$=p(T)G_0^-\left(1-R^{(t)}\right)\left[1-G_0^+\left(1-R^{(t)}\right)\right]. \quad (5)$$

Here $R^{(t)}$ refers to the probability that a randomly selected computer is infected at the time t. It means that at least one interaction originating from the computer has transmitted the virus before time t, resulting in the probability includes large number of events for a high-degree computer. Thus, we take into account the opposite event, which is that none of the interactions originating from the computer have transmitted the virus. This opposite event consists the following two situations: one is that all structural interactions of this computer are inactive ($1-P_L^{(t-1)}$), the other one is that the structural interactions of this computer are active, but connected to a virus-free computer ($u^{(t)}P_L^{(t-1)}$).

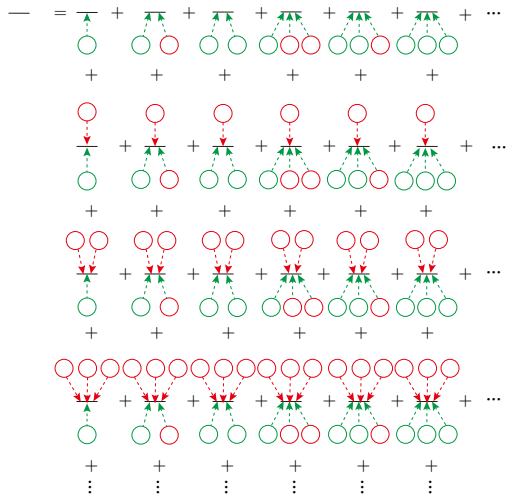


Fig. 4. Schematic diagram of the summation rule that a selected structural interaction is active when $p(T)=1$. The black solid lines represent active structural interaction. The red and the green dashed lines represent the negative and positive regulatory role, the red and the green circles represent inactive and active computers. This schematic diagram can be expressed as Eq. (5).

As shown in Fig. 5(a), a computer with degree k is not infected at the time t, means that its m structural interactions ($0\le m\le k$) are active at the time $t-1$ but are connected to the virus-free computers at the time t, and its $k-m$ structural interactions were inactive at the time $t-1$. The probability $1-R^{(t)}$ that a randomly selected computer is virus-free can be obtained by averaging the probability that none of the k structural interactions of this computer spread the virus. Therefore, the probability $R^{(t)}$ that a randomly selected computer is infected at the time t is

$$\begin{aligned}R^{(t)}&=1-\sum_{m=0}^{M}\sum_{k=m}^{M}p(k)\binom{k}{m}\left(u^{(t)}P_L^{(t-1)}\right)^m\left(1-P_L^{(t-1)}\right)^{k-m}\\&=1-\sum_{k=0}^{M}p(k)\sum_{m=0}^{k}\binom{k}{m}\left(u^{(t)}P_L^{(t-1)}\right)^m\left(1-P_L^{(t-1)}\right)^{k-m}\\&=1-\sum_{k=0}^{M}p(k)\left(1-P_L^{(t-1)}+u^{(t)}P_L^{(t-1)}\right)^k\\&=1-G_0\left(1-P_L^{(t-1)}+u^{(t)}P_L^{(t-1)}\right), \quad (6)\end{aligned}$$

where $u^{(t)}$ refers to the probability that a virus-free computer is reached along a randomly selected interaction at the time t. It means that the remaining structural interactions (the excess structural interactions) from the computer have not transmitted the virus. As shown in Fig. 5(b), similar to $R(t)$, the probability $u^{(t)}$ that a virus-free computer is reached along a randomly selected interaction at the time t is

$$\begin{aligned}u^{(t)}&=\sum_{m=0}^{M}\sum_{k=m}^{M}q(k)\binom{k}{m}\left(u^{(t)}P_L^{(t-1)}\right)^m\left(1-P_L^{(t-1)}\right)^{k-m}\\&=\sum_{k=0}^{M}q(k)\sum_{m=0}^{k}\binom{k}{m}\left(u^{(t)}P_L^{(t-1)}\right)^m\left(1-P_L^{(t-1)}\right)^{k-m}\\&=\sum_{k=0}^{M}q(k)\left(1-P_L^{(t-1)}+u^{(t)}P_L^{(t-1)}\right)^k\\&=G_1\left(1-P_L^{(t-1)}+u^{(t)}P_L^{(t-1)}\right). \quad (7)\end{aligned}$$

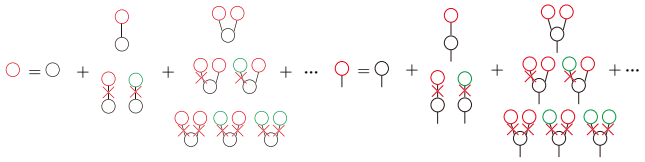


Fig. 5. (a) Schematic diagram of the summation rule that a randomly selected computer is virus-free. (b) Schematic diagram of the summation rule that a computer arriving along a randomly selected structural interaction is virus-free. The black circles represent the computers, the red and green circles represent the inactive and active computers. The black solid lines represent structural interactions, and the black solid lines with red crosses indicate the inactive structural interactions. The schematic can be respectively expressed as Eqs. (6) and (7).

To sum up, we obtain the following triadic percolation model about the computer virus:

$$\begin{aligned}P_L^{(t)}&=p(T)G_0^-\left(1-R^{(t)}\right)\left[1-G_0^+\left(1-R^{(t)}\right)\right],\\R^{(t)}&=1-G_0\left(1-P_L^{(t-1)}+u^{(t)}P_L^{(t-1)}\right),\\u^{(t)}&=G_1\left(1-P_L^{(t-1)}+u^{(t)}P_L^{(t-1)}\right). \quad (8)\end{aligned}$$

3. Analysis and calculation of percolation threshold

The percolation threshold constitutes a fundamental concept within percolation theory and assumes a crucial role in the comprehension of percolation phenomena.[44] In the context of a computer virus network, the presence of a giant component indicates a large-scale outbreak of the virus. The size of this giant component reflects the potential extent of the virus's spread across the network. The percolation threshold represents the critical point at which such a spread becomes possible. Beneath this threshold, a giant component does not exist, and the virus is unable to spread throughout the network.

However, above the threshold, a giant component is formed, enabling the virus to permeate the entire network. In the following analysis, we calculate the percolation threshold for a triadic percolation model to assess its implications for computer virus spreading.

Drawing on the fundamental principles of statistics and extensive long-term observations of computer virus incidents, the Poisson distribution could be a suitable model for simulating the initial infections of computers within the network.[45] The Poisson distribution has the capacity to describe the probability of a given number of events occurring within a fixed time or spatial interval, which is well-aligned with the nature of virus infections in a computer network. Consequently, as elaborated in Subsection 2.2.1, we posit that $p(k)$ and $\hat{P}_{\pm}(\hat{\kappa}^{\pm})$ respectively follow the Poisson distributions

$$p(k) = \frac{\langle k\rangle^{k}\exp(-\langle k\rangle)}{k!}, \tag{9}$$

$$\hat{P}_{\pm}(\hat{\kappa}^{\pm}) = \frac{\langle \hat{\kappa}^{\pm}\rangle^{\hat{\kappa}^{\pm}}\exp(-\langle \hat{\kappa}^{\pm}\rangle)}{\hat{\kappa}^{\pm}!}. \tag{10}$$

Substituting the above distributions into model (8), we have

$$\begin{aligned}
u^{(t)} &= G_1\left(1-P_L^{(t-1)}+u^{(t)}P_L^{(t-1)}\right)\\
&= \sum_k p(k)\frac{k}{\langle k\rangle}\left(1-P_L^{(t-1)}+u^{(t)}P_L^{(t-1)}\right)^{k-1}\\
&= \sum_k \frac{\langle k\rangle^{k}\exp(-\langle k\rangle)}{k!}\frac{k}{\langle k\rangle}\left(1-P_L^{(t-1)}+u^{(t)}P_L^{(t-1)}\right)^{k-1}\\
&= \exp(-\langle k\rangle)\sum_k \frac{1}{(k-1)!}\langle k\rangle^{k-1}\\
&\quad\times\left(1-P_L^{(t-1)}+u^{(t)}P_L^{(t-1)}\right)^{k-1}\\
&= \exp\left(-\langle k\rangle P_L^{(t-1)}+\langle k\rangle u^{(t)}P_L^{(t-1)}\right),
\end{aligned} \tag{11}$$

$$\begin{aligned}
R^{(t)} &= 1-G_0\left(1-P_L^{(t-1)}+u^{(t)}P_L^{(t-1)}\right)\\
&= 1-\sum_k p(k)\left(1-P_L^{(t-1)}+u^{(t)}P_L^{(t-1)}\right)^{k}\\
&= 1-\sum_k \frac{\langle k\rangle^{k}\exp(-\langle k\rangle)}{k!}\left(1-P_L^{(t-1)}+u^{(t)}P_L^{(t-1)}\right)^{k}\\
&= 1-\exp\left(-\langle k\rangle P_L^{(t-1)}+\langle k\rangle u^{(t)}P_L^{(t-1)}\right)\\
&= 1-\exp\left(-\langle k\rangle P_L^{(t-1)}+\langle k\rangle\left(1-R^{(t)}\right)P_L^{(t-1)}\right)\\
&= 1-\exp\left(-\langle k\rangle R^{(t)}P_L^{(t-1)}\right),
\end{aligned} \tag{12}$$

$$\begin{aligned}
P_L^{(t)} &= p(T)G_0^{-}\left(1-R^{(t)}\right)\left[1-G_0^{+}\left(1-R^{(t)}\right)\right]\\
&= p(T)\left[\sum_{\hat{\kappa}^-}\hat{P}_-(\hat{\kappa}^-)\left(1-R^{(t)}\right)^{\hat{\kappa}^-}\right]\\
&\quad\times\left[1-\sum_{\hat{\kappa}^+}\hat{P}_+(\hat{\kappa}^+)\left(1-R^{(t)}\right)^{\hat{\kappa}^+}\right]\\
&= p(T)\left[\sum_{\hat{\kappa}^-}\frac{\langle \hat{\kappa}^-\rangle^{\hat{\kappa}^-}\exp(-\langle \hat{\kappa}^-\rangle)}{\hat{\kappa}^-!}\left(1-R^{(t)}\right)^{\hat{\kappa}^-}\right]\\
&\quad\times\left[1-\sum_{\hat{\kappa}^+}\frac{\langle \hat{\kappa}^+\rangle^{\hat{\kappa}^+}\exp(-\langle \hat{\kappa}^+\rangle)}{\hat{\kappa}^+!}\left(1-R^{(t)}\right)^{\hat{\kappa}^+}\right]\\
&= p(T)\exp\left(-\langle \hat{\kappa}^-\rangle R^{(t)}\right)\\
&\quad\times\left[1-\exp\left(-\langle \hat{\kappa}^+\rangle R^{(t)}\right)\right].
\end{aligned} \tag{13}$$

According to Eq. (12), $R^{(t)}$ is a mapping of $P_L^{(t-1)}$, which can be expressed as $R^{(t)} = f(P_L^{(t-1)})$. Similarly, based on Eq. (13), $P_L^{(t-1)}$ is a mapping of $R^{(t-1)}$, represented as $P_L^{(t-1)} = g_{p(T)}(R^{(t-1)})$. By applying recursion, $R^{(t)}$ can be reduced to a one-dimensional mapping, expressed as

$$R^{(t)} = h_{p(T)}\left(R^{(t-1)}\right). \tag{14}$$

The specific form of Eq. (14) can be written as

$$\begin{aligned}
R^{(t)} &= 1-\exp\left[-\langle k\rangle R^{(t)}p(T)\exp(-\langle \hat{\kappa}^-\rangle R^{(t-1)})\right.\\
&\quad\left.\times\left(1-\exp(-\langle \hat{\kappa}^+\rangle R^{(t-1)})\right)\right].
\end{aligned} \tag{15}$$

It follows that the fixed point R^* of system (15) satisfies

$$\begin{aligned}
R^* &= 1-\exp\left[-\langle k\rangle R^* p(T)\exp\left(-\langle \hat{\kappa}^-\rangle R^*\right)\right.\\
&\quad\left.\times\left(1-\exp\left(-\langle \hat{\kappa}^+\rangle R^*\right)\right)\right].
\end{aligned} \tag{16}$$

Since equation (16) is a complicated transcendental equation, we use the graphical method to solve it. Let y equal the right-hand side of Eq. (16), i.e.,

$$\begin{aligned}
y &= 1-\exp\left[-\langle k\rangle R^* p(T)\exp\left(-\langle \hat{\kappa}^-\rangle R^*\right)\right.\\
&\quad\left.\times\left(1-\exp\left(-\langle \hat{\kappa}^+\rangle R^*\right)\right)\right].
\end{aligned} \tag{17}$$

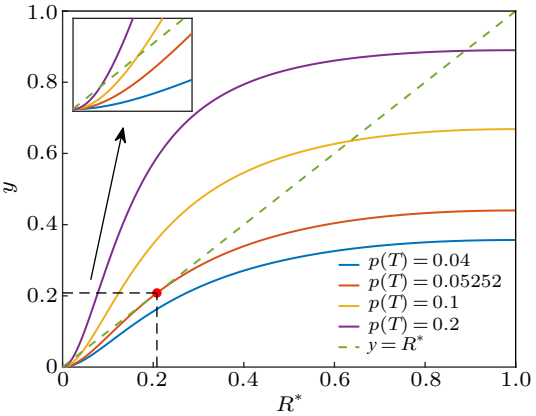


Fig. 6. The illustrations of y and R^* for different $p(T)$. The solid lines in different colors represent different $p(T)$-values. Among them, the red solid line ($p(T) = 0.05252$) and the diagonal $y = R^*$ exists a unique tangent point (red point), which is the critical value R_c. Here, the parameters $\langle k\rangle = 30$, $\langle \hat{\kappa}^+\rangle = 10$ and $\langle \hat{\kappa}^-\rangle = 1$. The inset in the figure is a specific enlarged view of y near 0.

In Fig. 6, we plot the relationship between y and R^*. The intersection of the solid and dotted line signifies the solution of the fixed point R^*. It can be observed that, given the parameters $\langle k\rangle = 30$, $\langle \hat{\kappa}^+\rangle = 10$ and $\langle \hat{\kappa}^-\rangle = 1$, when $p(T) = 0.02$ (illustrated by the solid blue line), the solution R^* of Eq. (17)

comprises only one trivial solution. When $p(T) = 0.05252$ (indicated by the solid red line), the solution R^* of Eq. (17) includes both a trivial solution and a non-trivial solution, with the latter being denoted as R_c. Notably, R_c corresponds to the tangent point (highlighted by a red dot) at which the red solid line intersects the dashed line. At this point, the slope of y is exactly equal 1. Increasing $p(T)$ further to 0.1 and 0.2 (represented by the solid yellow and purple line), the solution R^* of Eq. (17) consists of one trivial solution and two non-trivial solutions. Importantly, the slope of y at any point is intrinsically linked to its derivative at that very point, leading to the emergence of R_c precisely when the derivative of y equals 1.

We first take the derivative of y with respect to R^* as

$$\begin{aligned}\frac{\mathrm{d}y}{\mathrm{d}R^*} &= \langle k\rangle p(T)\exp\left[-\langle k\rangle R^* p(T)\exp\left(-\langle\hat{\kappa}^-\rangle R^*\right)\right.\\ &\times\left(1-\exp\left(-\langle\hat{\kappa}^+\rangle R^*\right)\right)\Big]\\ &\times\Big[\left(1-\langle\hat{\kappa}^-\rangle R^*\right)\exp\left(-\langle\hat{\kappa}^-\rangle R^*\right)\\ &+\left(R^*\left(\langle\hat{\kappa}^+\rangle+\langle\hat{\kappa}^-\rangle\right)-1\right)\\ &\times\exp\left[-\left(\langle\hat{\kappa}^+\rangle+\langle\hat{\kappa}^-\rangle\right)R^*\right]\Big]. \end{aligned}\tag{18}$$

It is found that

$$\left.\frac{\mathrm{d}y}{\mathrm{d}R^*}\right|_{R^*=0} = 0 < 1,$$

which implies that all y-curves originate below the diagonal line. As the parameter $p(T)$ increases, there exists a unique y-curve tangent to the diagonal line (i.e., the slope equals 1), the tangent point corresponds precisely to the unique nontrivial solution R_c. At this point, we get the percolation threshold T_c. Specifically, equation (18) = 1 leads to

$$\begin{aligned}1 &= \langle k\rangle p(T_c)\exp\left[-\langle k\rangle R_c p(T_c)\exp\left(-\langle\hat{\kappa}^-\rangle R_c\right)\right.\\ &\times\left(1-\exp\left(-\langle\hat{\kappa}^+\rangle R_c\right)\right)\Big]\\ &\times\Big[\left(1-\langle\hat{\kappa}^-\rangle R_c\right)\exp\left(-\langle\hat{\kappa}^-\rangle R_c\right)\\ &+\left(R_c\left(\langle\hat{\kappa}^+\rangle+\langle\hat{\kappa}^-\rangle\right)-1\right)\\ &\times\exp\left[-\left(\langle\hat{\kappa}^+\rangle+\langle\hat{\kappa}^-\rangle\right)R_c\right]\Big]. \end{aligned}\tag{19}$$

According to Eq. (16), it also has

$$\begin{aligned}R_c &= 1-\exp\left[-\langle k\rangle R_c p(T_c)\exp\left(-\langle\hat{\kappa}^-\rangle R_c\right)\right.\\ &\times\left(1-\exp\left(-\langle\hat{\kappa}^+\rangle R_c\right)\right)\Big]. \end{aligned}\tag{20}$$

We further obtain

$$p(T_c) = \frac{\ln(1-R_c)}{-\langle k\rangle R_c\exp\left(-\langle\hat{\kappa}^-\rangle R_c\right)\left(1-\exp\left(-\langle\hat{\kappa}^+\rangle R_c\right)\right)}.\tag{21}$$

Then, substituting Eq. (21) into Eq. (19), we could obtain equation related to R_c as

$$\frac{(1-R_c)\ln(1-R_c)}{-R_c\left(1-\exp\left(-\langle\hat{\kappa}^+\rangle R_c\right)\right)}\left[1-\langle\hat{\kappa}^-\rangle R_c+\left(\langle\hat{\kappa}^+\rangle R_c+\langle\hat{\kappa}^-\rangle R_c-1\right)\exp\left(-\langle\hat{\kappa}^+\rangle R_c\right)\right]-1=0.\tag{22}$$

Further, according to Eq. (22), we could calculate R_c, and then according to Eq. (21) the percolation threshold associated with $p(T)$ is given as follows:

(i) The linear relationship: when $p(T) = (1-\alpha)T$, the percolation threshold is

$$T_c = \frac{\ln(1-R_c)}{-\langle k\rangle(1-\alpha)R_c\exp\left(-\langle\hat{\kappa}^-\rangle R_c\right)\left(1-\exp\left(-\langle\hat{\kappa}^+\rangle R_c\right)\right)},\tag{23}$$

(ii) The nonlinear relationship: when $p(T) = CT/(DT+1)$, the percolation threshold is

$$T_c = \frac{\ln(1-R_c)}{C\left[-\langle k\rangle R_c\exp\left(-\langle\hat{\kappa}^-\rangle R_c\right)\left(1-\exp\left(-\langle\hat{\kappa}^+\rangle R_c\right)\right)\right]-D\ln(1-R_c)}.\tag{24}$$

According to Eqs. (22)–(24), an in-depth analysis of the percolation threshold is conducted within two distinct scenarios: the linear and nonlinear relationships of $p(T)$ associated with T. In each case, meticulous consideration is given to the impact of three crucial factors: the negative average degree $\langle\hat{\kappa}^-\rangle$ of structural interactions, the average degree $\langle k\rangle$ of computers and the positive average degree $\langle\hat{\kappa}^+\rangle$ of structural interactions. The relationships between the percolation threshold and the parameters $\langle\hat{\kappa}^-\rangle$, $\langle k\rangle$, and $\langle\hat{\kappa}^+\rangle$ are respectively illustrated in Figs. 7–9.

Figure 7 expresses the influence exerted by the negative average degree $\langle\hat{\kappa}^-\rangle$ on the percolation threshold T_c. In Fig. 7(a), $\langle k\rangle = 30$, the value of $\langle\hat{\kappa}^+\rangle$ is categorized into three cases: $\langle\hat{\kappa}^+\rangle = 10$ (circles), $\langle\hat{\kappa}^+\rangle = 20$ (squares), and $\langle\hat{\kappa}^+\rangle = 30$ (stars). In Fig. 7(b), $\langle\hat{\kappa}^+\rangle = 10$, the value of $\langle k\rangle$ splits into three cases: $\langle k\rangle = 30$ (circles), $\langle k\rangle = 50$ (squares), and $\langle k\rangle = 70$ (stars). It can be observed that as the negative average degree $\langle\hat{\kappa}^-\rangle$ increases, the percolation threshold T_c also increases. Significantly, in Fig. 7, when the transmission probability $p(T)$ is linear, the percolation threshold T_c and the negative average degree $\langle\hat{\kappa}^-\rangle$ display a linear correlation. In contrast, when $p(T)$ is nonlinear, they display a nonlinear correlation. The growth rate of percolation threshold T_c with the increase in $\langle\hat{\kappa}^-\rangle$ becomes progressively larger. In other words,

under the identical percolation threshold T_c, the negative average degree $\langle \hat{\kappa}^- \rangle$ associated with the nonlinear $p(T)$ is smaller than $\langle \hat{\kappa}^- \rangle$ associated with the linear $p(T)$. This implies that the role of prevention and control is often underestimated in practical applications when the transmission probability $p(T)$ is linear.

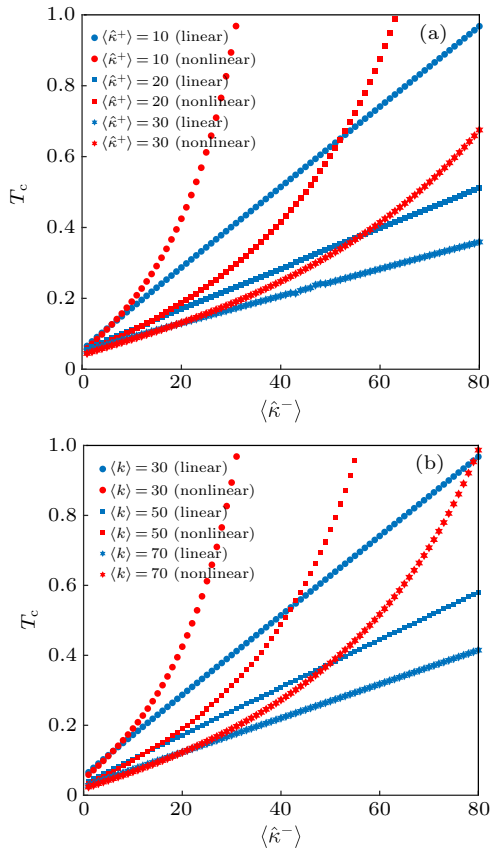


Fig. 7. Schematic representation of the percolation threshold as a function of the negative average degree $\langle \hat{\kappa}^- \rangle$ of the regulatory network. Red indicates the linear case and blue indicates the nonlinear case. The parameters of the function $p(T)$ are $\alpha = 0.2$, $C = 1$, and $D = 3$. (a) The average degree $\langle k \rangle = 30$, the positive average degree $\langle \hat{\kappa}^+ \rangle$ are respectively equal to 10 (circles), 20 (squares), 30 (stars). (b) The positive average degree $\langle \hat{\kappa}^+ \rangle = 10$, the average degree $\langle k \rangle$ are respectively equal to 30 (circles), 50 (squares), 70 (stars).

Figures 8 and 9 illustrate the influence of the average degree $\langle k \rangle$ and the positive average degree $\langle \hat{\kappa}^+ \rangle$ on the percolation threshold T_c. In Fig. 8(a), $\langle \hat{\kappa}^+ \rangle = 10$, the negative average degree $\langle \hat{\kappa}^- \rangle$ is associated with three cases: $\langle \hat{\kappa}^- \rangle = 1$ (circles), $\langle \hat{\kappa}^- \rangle = 5$ (squares), and $\langle \hat{\kappa}^- \rangle = 10$ (stars). In Fig. 8(b), $\langle \hat{\kappa}^- \rangle = 1$, $\langle \hat{\kappa}^+ \rangle$ aligns with the cases presented in Fig. 7(a). In Fig. 9(a), $\langle k \rangle = 30$, $\langle \hat{\kappa}^- \rangle$ is categorized into the same three cases as shown in Fig. 8(a). In Fig. 9(b), $\langle \hat{\kappa}^- \rangle = 1$, $\langle k \rangle$ is similarly divided into three cases, as illustrated in Fig. 7(b). From Figs. 8 and 9, a consistent and remarkable trend emerges: the percolation threshold T_c decreases as either the average degree $\langle k \rangle$ or the positive average degree $\langle \hat{\kappa}^+ \rangle$ increases. Furthermore, the rate of this decrease gradually decelerates, ultimately stabilizing at a lower level, irrespective of whether $p(T)$ is linear or nonlinear.

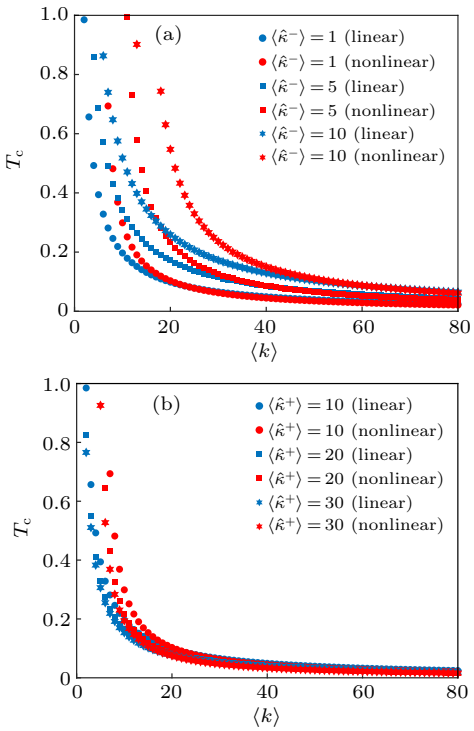


Fig. 8. Schematic representation of the percolation threshold as a function of the average degree $\langle k \rangle$ of the structural network. Red indicates the linear case and blue indicates the nonlinear case. The parameters of the function $p(T)$ are $\alpha = 0.2$, $C = 1$, and $D = 3$. (a) The positive average degree $\langle \hat{\kappa}^+ \rangle = 10$, while the negative average degree $\langle \hat{\kappa}^- \rangle$ are respectively equal to 1 (circles), 5 (squares), 10 (stars). (b) The negative average degree $\langle \hat{\kappa}^- \rangle = 1$, the positive average degree $\langle \hat{\kappa}^+ \rangle$ is respectively equal to 10 (circles), 20 (squares), 30 (stars).

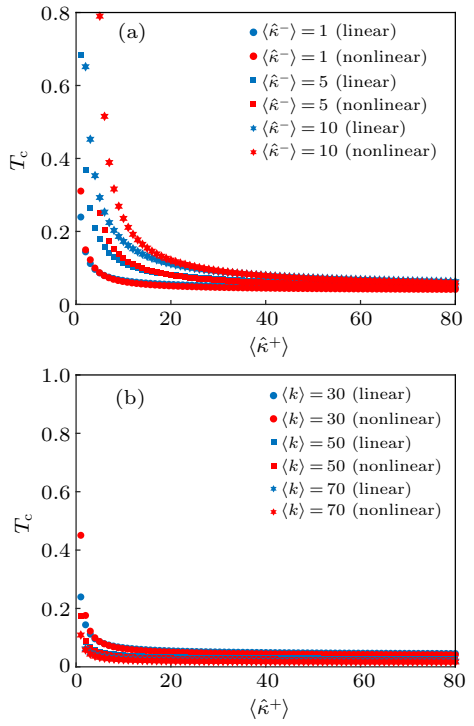


Fig. 9. Schematic representation of the percolation threshold as a function of the positive average degree $\langle \hat{\kappa}^+ \rangle$ of the regulatory network. Red indicates the linear case and blue indicates the nonlinear case. The parameters of the function $p(T)$ are $\alpha = 0.2$, $C = 1$, and $D = 3$. (a) The average degree $\langle k \rangle = 30$, the negative average degree $\langle \hat{\kappa}^- \rangle$ are respectively equal to 1 (circles), 5 (squares), 10 (stars). (b) The negative average degree $\langle \hat{\kappa}^- \rangle = 1$, the average degree $\langle k \rangle$ is respectively equal to 30 (circles), 50 (squares), 70 (stars).

In conclusion, we have analytically determined the percolation threshold T_c for two distinct cases ($p(T)$ is linear or nonlinear) in the preceding sections and further analyzed the influence of parameters, including the negative average degree $\langle \hat{\kappa}^- \rangle$, the average degree $\langle k \rangle$ and the positive average degree $\langle \hat{\kappa}^+ \rangle$ on the percolation threshold. Our results indicate that the percolation threshold T_c is almost equally influenced by $\langle k \rangle$ and $\langle \hat{\kappa}^+ \rangle$, regardless of whether $p(T)$ is linear or nonlinear. However, there is a huge difference between the percolation threshold T_c as a function of $\langle \hat{\kappa}^- \rangle$ when $p(T)$ is linear *versus* nonlinear. Specifically, when $p(T)$ is linear, T_c and $\langle \hat{\kappa}^- \rangle$ are linearly related, but when $p(T)$ is nonlinear, T_c and $\langle \hat{\kappa}^- \rangle$ display a clear nonlinear relationship. This is evidenced by the fact that T_c increases more rapidly with $\langle \hat{\kappa}^- \rangle$ in the nonlinear case. $\langle \hat{\kappa}^- \rangle$ in the nonlinear case is smaller than in the linear case at the same T_c. In essence, the linear case underestimates the role of computer virus prevention and control, resulting in a waste of resources in practice.

In the above section, we analytically derived the percolation threshold T_c, but the dynamics above threshold T_c are relatively complex. Next, we will present qualitative results obtained through simulation.

4. The dynamics of triadic percolation above the threshold

In this part, we investigate the effect of three parameters, the average degree $\langle k \rangle$, the positive average degree $\langle \hat{\kappa}^+ \rangle$, and the negative average degree $\langle \hat{\kappa}^- \rangle$, on the triadic percolation dynamics above the percolation threshold T_c, considering both linear and nonlinear cases for $p(T)$.

Figures 10 and 11 respectively illustrate the influence of the natural transmission probability T on triadic percolation dynamics under varying values of the average degree $\langle k \rangle$ and the positive average degree $\langle \hat{\kappa}^+ \rangle$. The transmission probability $p(T)$ is linear in Figs. 10(a), 11(a) and nonlinear in Figs. 10(b), 11(b). In Fig. 10, the values of $\langle k \rangle$ are 30 (blue circle), 60 (red triangle), and 90 (yellow diamond). In Fig. 11, the values of $\langle \hat{\kappa}^+ \rangle$ are 2 (blue circle), 6 (red triangle), and 10 (yellow diamond). It is observed that in both two cases of $p(T)$, above the percolation threshold T_c, changes in $\langle k \rangle$ or $\langle \hat{\kappa}^+ \rangle$ do not affect the dynamical complexity, the number of non-zero solutions, and they all tend to one non-zero solution. However, these changes have an impact on the final size R_∞: as $\langle k \rangle$ or $\langle \hat{\kappa}^+ \rangle$ increases, R_∞ also increases, but when $\langle \hat{\kappa}^+ \rangle$ reaches a large value, the dynamics do not continue to grow. When all parameter values are identical, R_∞ in the nonlinear case is significantly smaller than R_∞ in the linear case.

Figure 12 demonstrates the impact of the natural transmission probability T on triadic percolation dynamics across different values of the negative average degree $\langle \hat{\kappa}^- \rangle$. The transmission probability $p(T)$ is linear in Fig. 12(a) and nonlinear in Fig. 12(b). The values of $\langle \hat{\kappa}^- \rangle$ are 0.2 (blue circle), 1 (red triangle), and 1.8 (yellow diamond). In terms of the final size R_∞: above the percolation threshold T_c, regardless of

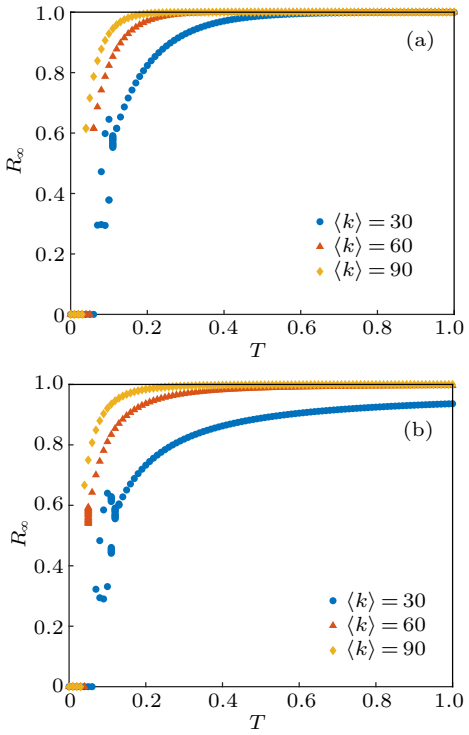


Fig. 10. Schematic representation of the final size R_∞ as a function of the natural transmission probability T with $\langle \hat{\kappa}^+ \rangle = 10$ and $\langle \hat{\kappa}^- \rangle = 1$. The average degree $\langle k \rangle$ is respectively equal to 30 (blue circle), 60 (red triangle), and 90 (yellow diamond). (a) $p(T)$ is linear. (b) $p(T)$ is nonlinear.

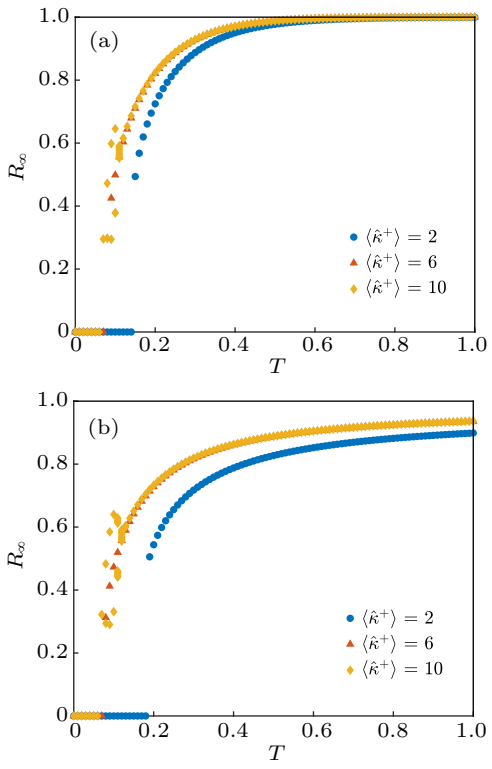


Fig. 11. Schematic representation of the final size R_∞ as a function of the natural transmission probability T with $\langle k \rangle = 30$ and $\langle \hat{\kappa}^- \rangle = 1$. The positive average degree $\langle \hat{\kappa}^+ \rangle$ is respectively equal to 2 (blue circle), 6 (red triangle), and 10 (yellow diamond). (a) $p(T)$ is linear. (b) $p(T)$ is nonlinear.

whether $p(T)$ is linear or nonlinear, as $\langle\hat{\kappa}^{-}\rangle$ increases (for instance, from 0.2 to 1), the final size R_∞ decreases with the natural transmission probability T. Notably, when $\langle\hat{\kappa}^{-}\rangle$ increases to a relatively large value (such as 1.8), multiple solutions will appear. At this time, some of them may be larger than those of the previous group. In terms of the solution number of final size R_∞: for smaller values of $\langle\hat{\kappa}^{-}\rangle$, such as 0.2 and 1, the number of R_∞ is ultimately one. When $\langle\hat{\kappa}^{-}\rangle$ continues to increase to 1.8, there is a multi-solution process in the middle as T changes for the linear case. For the nonlinear case, there is a multi-solution process in the middle, and ultimately it always remains a case of two solutions. Obviously, in contrast to linear case, which converges to a single solution, the nonlinear case exhibits increased complexity, often resulting in the coexistence of two solutions as the parameter T increases. The nonlinear case increases the complexity of the solutions.

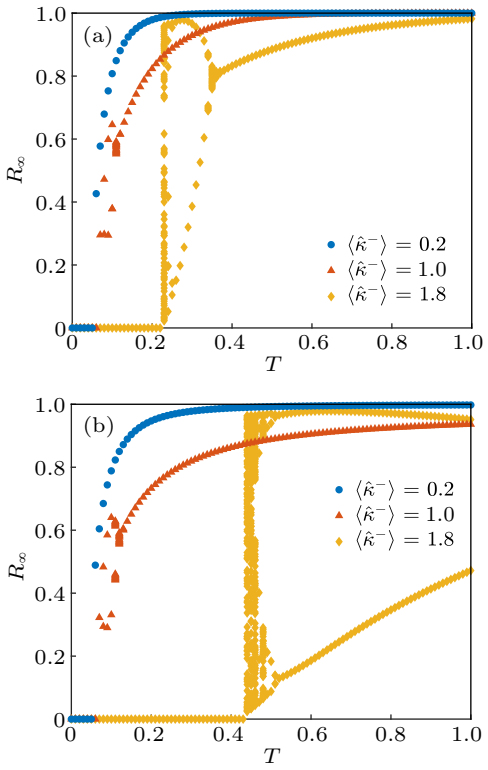


Fig. 12. Schematic representation of the final size R_∞ as a function of the natural transmission probability T with $\langle k\rangle = 30$ and $\langle\hat{\kappa}^{+}\rangle = 10$. The negative average degree $\langle\hat{\kappa}^{-}\rangle$ is respectively equal to 0.2 (blue circle), 1 (red triangle), and 1.8 (yellow diamond). (a) $p(T)$ is linear. (b) $p(T)$ is nonlinear.

Figures 10–12 show the variations of the final size R_∞ with respect to the transmission probability T. As we mentioned, the triadic percolation model is capable of capturing the changes in the final size over time. Therefore, we present two plots of the size R over time in Fig. 13 where the parameters correspond to the above Figs. 10–12. The parameters $\langle k\rangle = 30$ and $\langle\hat{\kappa}^{+}\rangle = 10$, in Fig. 13(a), $T = 0.2$, $\langle\hat{\kappa}^{-}\rangle = 1$, in Fig. 13(b), $T = 0.8$, $\langle\hat{\kappa}^{-}\rangle = 1.8$. Figure 13(a) demonstrates that both solution numbers tend to one in the two cases of $p(T)$. In contrast, figure 13(b) shows that the solution number tends to one in the linear case, but eventually tends to two in the nonlinear case. In a word, the nonlinear nature of $p(T)$ exerts a significant impact on the dynamic behavior of the size R of the computer virus spreading.

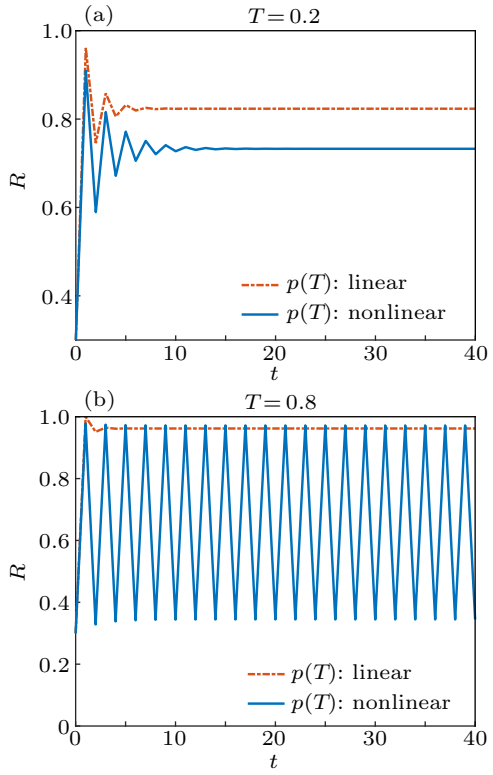


Fig. 13. Plots of the size R over time with $\langle k\rangle = 30$ and $\langle\hat{\kappa}^{+}\rangle = 10$. We assume that the initial state of the iteration is $R_0 = 0.3$. The dashed orange line represents the linear case and the solid blue line represents the nonlinear case. (a) $T = 0.2$, $\langle\hat{\kappa}^{-}\rangle = 1$. (b) $T = 0.8$, $\langle\hat{\kappa}^{-}\rangle = 1.8$.

In addition, the simulation presented in Figs. 10–12 validates the previously analyzed relationship between the percolation threshold T_c and the parameters $\langle\hat{\kappa}^{-}\rangle$, $\langle k\rangle$, and $\langle\hat{\kappa}^{+}\rangle$. Specifically, the percolation threshold T_c is the T value at which the first non-zero R_∞ emerges. We observed that in Figs. 10 and 11, as the average degree $\langle k\rangle$ or the positive average degree $\langle\hat{\kappa}^{+}\rangle$ increases, the T value for the initial occurrence of non-zero R_∞ decreases. However, in Fig. 12, as the negative average degree $\langle\hat{\kappa}^{-}\rangle$ increases, the T value for the initial occurrence of non-zero R_∞ increases. These observations are consistent with the conclusions drawn in Section 3 and enhance the consistency and validity of the findings.

In summary, in terms of the final size R_∞: R_∞ will increase with the increase of the natural transmission probability T, the average degree $\langle k\rangle$ or the positive average degree $\langle\hat{\kappa}^{+}\rangle$, and decrease with the increase of the negative average degree $\langle\hat{\kappa}^{-}\rangle$, regardless of whether $p(T)$ is linear or nonlinear. Furthermore, the final size R_∞ is typically smaller in the nonlinear case. In terms of the solution number of the final size R_∞, we conclude that as $\langle\hat{\kappa}^{-}\rangle$ increases, the solution number of the final size R_∞ will present a more complex multi-solution situation in the nonlinear case.

5. Conclusion

The triadic percolation not only describes the dynamic behaviors over time, but also incorporates the effects of regulatory influences. In this work, we have applied the triadic percolation model to the study of computer virus spreading dynamics and deeply explored the nonlinear characteristics of transmission probability. Through detailed mathematical analysis, we derived the triadic percolation computer virus spreading model (Eq. (8)) and the percolation threshold (Eqs. (23) and (24)) that consider the nonlinear nature of the transmission probability. Regarding the triadic threshold, as depicted in Fig. 7, it is substantially influenced by nonlinearity and exhibits pronounced nonlinear traits as $\langle \hat{\kappa}^{-} \rangle$ varies. Under identical parameter settings, the nonlinear percolation threshold is relatively larger. Furthermore, we conducted simulations to observe the changes in the final size of percolation dynamics (refer to Figs. 10–12). These simulations indicate that by reducing $\langle k \rangle$ and $\langle \hat{\kappa}^{+} \rangle$, and increasing $\langle \hat{\kappa}^{-} \rangle$, the final size of computer virus spread can be effectively controlled. In addition, to prevent the emergence of multiple solutions, which can complicate prevention and control efforts, we advocate for enhanced governmental intervention to mitigate excessive negative regulation.

In conclusion, we proposed a computer virus spreading model predicated on triadic percolation. This model comprehensively incorporates the nonlinear characteristics of the transmission probability and the regulatory impacts, offering novel perspectives and strategies for the prevention of computer virus epidemics. Unfortunately, our results have not yet been substantiated with empirical data. To thoroughly assess the precision and practicality of the model, we intend to validate and refine it using real-world data in forthcoming research endeavors.

Acknowledgements

Project supported by the National Natural Science Foundation of China (Grant Nos. 12101573 and 12022113) and the Fundamental Research Program of Shanxi Province, China (Grant Nos. 20210302124381, 202203021211213, and 20210302123018).

References

[1] Cohen F 1987 *Comput. Secur.* **6** 22
[2] Balthrop J, Forrest S, Newman M E and Williamson M M 2004 *Science* **304** 527
[3] Essam J W 1980 *Rep. Prog. Phys.* **43** 833
[4] Stauffer D and Aharony A 2018 *Introduction to percolation theory*, 2nd Edn. (London: Taylor & Francis) pp. 1–192
[5] Sun H L and Bianconi G 2021 *Phys. Rev. E* **104** 034306
[6] Li M, Liu R R, Lü L Y, Hu M B, Xu S Q and Zhang Y C 2021 *Phys. Rep.* **907** 1
[7] Zhu J C and Wang L W 2022 *Chin. Phys. B* **31** 068904
[8] Broadbent S R and Hammersley J M 1957 *Math. Proc. Cambridge Philos. Soc.* **53** 629
[9] Moore C and Newman M E 2000 *Phys. Rev. E* **62** 7059
[10] Meyers L 2007 *Bull. Am. Math. Soc.* **44** 63
[11] Newman M E 2002 *Phys. Rev. E* **66** 016128
[12] Cardy J L and Grassberger P 1985 *J. Phys. A Math. Gen.* **18** 267
[13] Chang L L, Gong W, Jin Z and Sun G Q 2022 *Siam J. Appl. Math.* **82** 1764
[14] Sun G Q, He R Z, Hou L F, Gao S P, Luo X F, Liu Q H, Zhang Y C and Chang L L 2024 *Europhys. Lett.* **147** 12001
[15] Xie J R, Meng F H, Sun J C, Ma X, Yan G and Hu Y Q 2021 *Nat. Hum. Behav.* **5** 1161
[16] Palmieri F 2012 *J. Syst. Softw.* **85** 2559
[17] Liu Y, Wei B, Wang Z and Deng Y 2015 *Phys. Lett. A* **379** 2795
[18] Mann P, Smith V A, Mitchell J B and Dobson S 2021 *Phys. Rev. E* **104** 024303
[19] Shang Y 2021 *Chaos* **31** 053117
[20] Liu S M, Bai Z G and Sun G Q 2023 *Nonlinearity* **36** 5699
[21] Luo X F and Jin Z 2020 *Commun. Nonlinear Sci. Numer. Simul.* **91** 105363
[22] Sun H L, Radicchi F, Kurths J and Bianconi G 2023 *Nat. Commun.* **14** 1308
[23] Millán A P, Sun H, Torres J J and Bianconi G 2024 *Pans Nexus* **3** 270
[24] Raza A, Arif M S, Rafiq M, Bibi M, Naveed M, Iqbal M U, Butt Z, Naseem H A and Abbasi J N 2019 *Cmes-Comp. Model Eng.* **120** 445
[25] Dubey V P, Kumar R and Kumar D 2020 *Chaos, Solitons and Fractals* **133** 109626
[26] Zarin R, Khaliq H, Khan A, Ahmed I and Humphries U W 2023 *Csymmetry* **15** 621
[27] Han X and Tan Q L 2010 *Appl. Math. Comput.* **217** 2520
[28] Murray W H 1988 *Icomput. Secur.* **7** 139
[29] He R Z, Luo X F, Asamoah J K K, Zhang Y X, Li Y H, Jin Z and Sun G Q 2023 *J. Math. Biol.* **87** 29
[30] Luo X F, Sun G Q, He R Z, Jin Z, Asamoah J K K, Xue Y K and Chang L L 2024 *Chaos* **34** 073114
[31] Mishra B K and Saini D 2007 *Appl. Math. Comput.* **187** 929
[32] Zhu Q Y, Yang X F and Ren J G 2012 *Commun. Nonlinear Sci. Numer. Simul.* **17** 5117
[33] Ren J G, Yang X F, Zhu Q Y, Yang L X and Zhang C M 2012 *Nonlinear Anal-Real* **3** 376
[34] Zarin R, Khaliq H, Khan A, Khan D, Akgül A and Humphries U W 2022 *Results Phys.* **33** 105130
[35] Singh J, Kumar D, Hammouch Z and Atangana A 2018 *Appl. Math. Comput.* **316** 504
[36] Gan C Q, Feng Q D, Zhu Q Y, Zhang Z F, Zhang Y S and Xiang Y 2020 *Nonlinear Dyn.* **100** 1725
[37] Lefebvre M 2020 *Atti della Accademia Peloritana dei Pericolanti-Classe di Scienze Fisiche, Matematiche e Naturali* **98** 3
[38] Yang F F and Zhang Z Z 2021 *AIMS Math.* **6** 4083
[39] Gao Y L, Yu H B, Zhou J, Zhou Y Z and Chen S M 2023 *Chin. Phys. B* **32** 098902
[40] Avcı D and Soytürk F 2023 *J. Comput. Appl. Math.* **419** 114740
[41] Yang L X and Yang X F 2015 *Nonlinear Dyn.* **82** 85
[42] Gan C Q, Yang X F, Liu W P, Zhu Q Y and Zhang X L 2013 *Appl. Math. Comput.* **4222** 265
[43] d'Onofrio A, Manfredi P and Salinelli E 2007 *Theor. Popul Biol.* **71** 301
[44] Newman M 2018 *Networks*, 2nd Edn. (Oxford University Press) pp. 569–602
[45] Kondakci S 2008 *Simul. Modell. Pract. Theory* **16** 571